Journal of Molecular Graphics and Modelling 29 (2010) 565–572

Contents lists available at ScienceDirect

Journal of Molecular Graphics and Modelling

journal homepage: www.elsevier.com/locate/JMGM

Dimerization of the AtoC response regulator and modelling of its binding to DNA

G. Papadopoulos [a], A.I. Grigoroudis [b], D.A. Kyriakidis [b,c,*]

[a] Department of Biochemistry & Biotechnology, University of Thessaly Ploutonos 26 & Aeolou, Larisa, GR-41221, Greece
[b] Laboratory of Biochemistry, Department of Chemistry, Aristotle University of Thessaloniki, GR-54124, Greece
[c] National Hellenic Research Foundation, 48 Vas. Constantinou Ave, GR-11635, Athens, Greece

ARTICLE INFO

Article history:
Received 19 April 2010
Received in revised form 12 October 2010
Accepted 18 October 2010
Available online 23 October 2010

Keywords:
AtoC modelling
DNA modeling
AtoC oligomerization
AtoC–DNA complex
Molecular dynamics simulations

ABSTRACT

Bacterial signal transduction systems can be viewed as an entity of multi-sensory and output domains, whereas the functions of response regulators play a pivotal role in the complex network interactions. One crucial property among response regulators functions is their oligomerization and subsequent binding to DNA. The AtoS–AtoC two component system, functionally modulated by various agents, influences fundamental cellular processes such as short-chain fatty acid catabolism and poly-(R)-3-hydroxybutyrate biosynthesis in *Escherichia coli*. Among the already reported characteristic properties, AtoC binds to a specific site, a palindromic repeat of 20 nucleotides within the *atoDAEB* promoter. Since experimental structures of AtoC or its complex with DNA are not yet available, an almost complete homology model of AtoC and of its putative entity as a dimer is constructed for this study, as well as a model of its binding to its target DNA sequence. The latter is associated with large conformational changes, as shown by molecular dynamics simulations. Subsequent biochemical study, including cross-linking via chemical agents, revealed the ability of AtoC to form oligomers *in vitro*.

1. Introduction

Sophisticated regulatory mechanisms in bacteria require components able to sense environmental or metabolic stimuli and trigger the appropriate response by activating gene expression. Such trans-activators are usually the latter parts of two-component signal transduction systems that typically consist of a sensor histidine kinase and a response regulator [27,32].

AtoSC is the two-component regulatory system that activates transcription of the *atoDAEB* operon genes in *Escherichia coli*. The *atoDAEB* expression, highly inducible by acetoacetate, is essential for the catabolism of short-chain fatty acids [9,20] while *atoSC* expression is reportedly related to various cell functions [19]. Additionally, the modulation of the poly-hydroxybutyrate (cPHB) biosynthesis in *E. coli* by AtoC has already been demonstrated [28], as well as the spermidine [29] or histamine [13] effects on this process attribute a phenomenal, more critical metabolic role to the *ato* regulon. Inducer response is ultimately carried out by the AtoC transcription factor, an NtrC-NifA type, bacterial transcriptional regulator of the σ^{54}-RNA polymerase holoenzyme [14,23].

Transcriptional activation by σ^{54}-operating bacterial regulators usually requires their oligomerization and cooperative binding to DNA. These characteristic properties are stimulated by ATP-dependent phosphorylation ([14,36] and references therein) and correspond to their structural determinants. A typical alignment of proteins belonging to this category reveals three characteristic conserved domains, i.e. the N-terminal receiver domain, containing their phosphorylation site, the central σ^{54}-RNA polymerase holoenzyme and the Helix–Turn–Helix (HTH) DNA-binding domain. Phosphorylation of the N-terminal receiver domain seems to govern activities corresponding to other domains, like oligomerization of the central domain and cooperative DNA-binding of the output domain, through both inter- and intra-molecular interactions [35].

AtoC, like its well-characterised counterparts has already been shown to possess ATPase activity that is phosphorylation-dependent and stimulated by site-specific DNA-binding [6,31,5]. Both the *in vitro* DNA binding data and *in vivo* Chromatin Immunoprecipitation (ChIP) analyses demonstrated that recombinant AtoC binds upstream the predicted *atoDAEB* transcription start sites [17]. The sequence of the inverted palindrome, comprising the AtoC binding site, conforms to a 20 bp-consensus and its location coincides with the relative positioning of other enhancer-like elements present in σ^{54}-dependent promoters [23]. Additional experimental data verified the participation of Integration Host Factor and the σ^{54}-RNA polymerase holoenzyme in the transcription of the *atoDAEB* promoter, as we expected following compilation and analysis

* Corresponding author at: Laboratory of Biochemistry, Department of Chemistry, Aristotle University of Thessaloniki, GR-54124 Thessaloniki, Greece.
Tel.: +30 2310997771; fax: +30 2310997689.
E-mail address: kyr@chem.auth.gr (D.A. Kyriakidis).

1093-3263/$ – see front matter © 2010 Elsevier Inc. All rights reserved.
doi:10.1016/j.jmgm.2010.10.004

of a large volume of σ^{54}-dependent bacterial promoter sequences [2].

According to the above similarities, it is evident that the structural determinants and functions of AtoC might be strongly related to its putative oligomerization state and to the way it binds to the DNA palindrome. Neither can be studied in atomistic detail prior to the determination of the 3D-structures of AtoC (monomer or dimer) or the DNA palindrome bound to AtoC. Shorn of to-date experimentally derived 3D high resolution structural data, in this work we attempt modelling the above molecules and their putative complexes providing, thus, a starting point for further biochemical analyses and considerations. Besides we provide for the first time additional experimental evidence of the AtoC oligomerization activity.

2. Methods

2.1. Modelling AtoC and its dimer

AtoC has a length of 454 amino acids. A homology model of AtoC aa 6–393 has been provided by http://swissmodel.expasy.org/SWISS-MODEL.html [26], based on the crystal structure of the σ^{54} activator from *Aquifex aeolicus* [Protein Data Bank (PDB):1ny5]. Local alignment using http://www.ch.embnet.org/software/LALIGN_form.html (Lalign server, [7]) resulted in a sequence identity of 43% and a similarity score of 837 with blosum62 and gap-open/ext: −14/−4. This model has been energy minimized and equilibrated for 2.4 ns with molecular dynamics simulation (MDS). The quality of this model has been evaluated using http://www.sbc.su.se/~bjornw/ProQ/ProQ.cgi (ProQ server, [30]) using as input the model coordinates and the Psipred [10] prediction of the secondary structure, resulting to an LGscore of 4.836 (extremely good model) and a MaxSub of 0.420 (fairly good model). An alignment of the secondary structure as predicted by Psipred and that of the model is shown below.

```
Conf:  99999286779999999997389719982999999998433899799981668999989 9
Pred:  CEEEEECCHHHHHHHHHHHHHCCCEEEEECCHHHHHHHHHCCCCCEEEEECCCCCCCHHH
Model: CEEEECCCHHHHHHHHHHHHHHCCEEECCCCHHHHHHHHHHCCCEEEEEECCCCCCCHH
  AA:  RILIVDDEDNVRRMLSTAFALQGFETHCANNGRTALHLFADIHPDVVLMDIRMPEMDGIK
          10        20        30        40        50        60

Conf:  99999833999938999426997789999864523122599996679999999997643 3
Pred:  HHHHHHHCCCCCCEEEEECCCCHHHHHHHHHCCCCCCCCCCCCHHHHHHHHHHHHHHHH
Model: HHHHHHHHCCCCEEEEEECCCCHHHHHHHHHCCCCEEEEECCCHHHHHHHHHHHHHHHH
  AA:  ALKEMRSHETRTPVILMTAYAEVETAVEALRCGAFDYVIKPFDLDELNLIVQRALQLQSM
          70        80        90       100       110       120

Conf:  99999987832047888896214988999999997760689918885899863889999 9
Pred:  HHHHHHHHHHHHCCCCCCCCCCCCHHHHHHHHHHHHHHHCCCCCEEEECCCCCCHHHHHHH
Model: HHHHHHHHHHHHCCCCCCCCCCCCHHHHHHHHHHHHHHHCCCCCEEEECCCCCCCHHHHHH
  AA:  KKEIRHLHQALSTSWQWGHILTNSPAMMDICKDTAKIALSQASVLISGESGTGKELIARA
          130       140       150       160       170       180

Conf:  870499999992000157889504775302843465769888965455640898020002
Pred:  HHHCCCCCCCCCEEECCCCCCCHHHHHHHCCCCCCCCCCCCCCCCCCEEECCCCEECCCC
Model: HHHCCCHHCCEEEEEEECCCCHHHHHHHHHCCCCCCCCCCCCCCCCCHHHHHCCEEEEEEE
  AA:  IHYNSRRAKGPFIKVNCAALPESLLESELFGHEKGAFTGAQTLRQGLFERANEGTLLLDE
          190       200       210       220       230       240

Conf:  589990135789775513937846797236502889934690589989809995111110
Pred:  CCCCCHHHHHHHHHHHHCCEEEECCCCCEEEEEEEEEECCCCCHHHHHHCCCCCCCCCCC
Model: CCCCCHHHHHHHHHHHHHEEECCCCCCCCEEECCEEEEEECCCHHHHHHCCCCHHHHHH
  AA:  IGEMPLVLQAKLLRILQEREFERIGGHQTIKVDIRIIAATNRDLQAMVKEGTFREDLFYR
          250       260       270       280       290       300

Conf:  131113799898887899999999999988770999999999999988649999848898
Pred:  CCCCCCCCCCCCCCCCCHHHHHHHHHHHHHHHHCCCCCCCCHHHHHHHHCCCCCCCHHHH
Model: HCCEEEEECCCCCCCCHHHHHHHHHHHHHHHHHCCCCCCCCCHHHHHHHHCCCCCCCHHH
  AA:  LNVIHLILPPLRDRREDISLLANHFLQKFSSENQRDIIDIDPMAMSLLTAWSWPGNIREL
          310       320       330       340       350       360

Conf:  679999878269994289999942237 7
Pred:  HHHHHHHHHHCCCCCCCCCCCCCCCCC
Model: HHHHHHHHHHCCCCCCCCCCCCCCCHH
  AA:  SNVIERAVVMNSGPIIFSEDLPPQIRQP
          370       380       390
```

The major part (aa 433–452) of the rest (aa 394–454) has been identified by BLAST searches over the conserved domain database as a putative DNA-binding domain. Region 394–454 has been modelled by threading according to the crystal structure of the factor for inversion stimulation from *E. coli* (PDB:1fip, Sequence Identity: 30%) using http://www.sbg.bio.ic.ac.uk/phyre [11]. The above region will be referred to as the "DNA binding domain (DBD)". The resulted merged structure has been used as a starting model for further energy minimization and equilibration (250 ps) with all atom Molecular Dynamics Simulation (MDS). Equilibration has been performed in spherical boundary conditions, in explicit water with counter ions and Langevin thermostat at 300 K using the MDS software "namd2" [22] and the CHARMM27 force field for proteins and nucleic acids. If not explicitly stated, the same simulation protocol has been applied for all simulations in this work. The systems have been considered as reached equilibrium, if the RMSD fluctuations do not rise monotonically at least for 1 ns.

A dimer for the σ interaction domain of the AtoC model has been constructed using the PQS server (http://www.ebi.ac.uk/msd-srv/pqs/) for PDB:1ny5. A dimer of the DBD has been also constructed separately using the docking software HEX [25]. Afterwards, the connecting arm has been inserted and structurally modified in order to obtain a closed AtoC dimer, which has been

further minimized and equilibrated with MDS for 2 ns. The properties of the dimer interface have been calculated by FastContact [3] and ProtorP [24]. The DCOMPLEX [15] program has been used to calculate protein–protein binding energies and DDNA2 [34] for protein–DNA.

2.2. Modelling DNA (−146 to −106)

A starting B-DNA model for the target sequence of AtoC binding has been provided by server http://www.scfbio-iitd.res.in/software/drugdesign/bdna.jsp [1] using as input the following palindrome:

```
-146                                    -106
   1       10        20          30        40
   GCTATGCAGAAATTTGCACA G TGCGCAATTTTCTGCATAGC
   CGATACGTCTTTAAACGTGT C ACGCGTTAAAAGACGTATCG
```

The resulted B-DNA structure has been further energy minimized and equilibrated for 5.6 ns in cylindrical boundary conditions. All other simulation details are as mentioned in the case of AtoC.

2.3. Modelling the complex B-DNA–AtoC

The AtoC–DNA interaction has been modelled by docking the DBD to our B-DNA model using the docking software HEX [25]. Among the complexes proposed by the program, four have been chosen as those satisfying the condition that positions −140, −121 and −111 might be important for AtoC binding [17]. After energy minimization and equilibration (∼18 ns each) of the four complexes the one with minimum protein–DNA interaction energy has been adopted as the model representing the AtoC–DNA interaction.

The geometrical properties of the three B-DNA models (starting model, equilibrated before AtoC binding, equilibrated after AtoC binding) have been calculated using the program 3DNA [33].

Molecular graphics images of the models were produced using the programs VMD [8] and the UCF Chimera [21].

2.4. In vitro cross-linking of purified AtoC

Purified His_{10}-AtoC were cross-linked for various time points (5, 10, 20 and 30 min) at 25 °C with 0.1% (v/v) glutaraldehyde in 20 mM HEPES–KOH, pH 7.9, 0.2 mM EDTA, 0.1 M NaCl, 20% (v/v) glycerol and 0.5 mM DTT, as previously described [4]. The reaction volume was 25 μl and the cross-linking was terminated by addition of SDS-PAGE loading buffer and boiling for 3 min. The complexes were analyzed by SDS-PAGE on 8.5% (w/v) gels and immunoblotting analysis was performed using the His-probe antibody against the histidine-tag, purchased by Santa Cruz Biotechnology, Inc. "ProSieve Color Protein Markers", purchased by Lonza Group, Switzerland, were used to determine molecular weights.

3. Results

3.1. Properties of the AtoC model

In order to understand the mechanism of AtoC regulatory function in the expression of the *atoDAEB* operon in *E. coli*, an almost complete model (6–454) of its structure has been constructed (Fig. 1). According to our model the aa 6–381 domain bears the same structural elements as its template, the σ^{54} activator from *A. aeolicus* classified in SCOP as an α/β protein. The secondary structure of the AtoC model is shown in Fig. 2 (σ interaction domain part in yellow, DBD in cyan). Region 382–392 (green) probably corresponds to a structure-less arm providing both DBDs in the dimer with some degrees of freedom in order to adopt a suitable configuration for DNA binding.

Fig. 1. Model of an AtoC monomer.

3.2. Properties of the AtoC dimmer model

Structural details concerning putative AtoC dimerization might give a new insight to its potential oligomerization function. The

```
MTAINRILIVDDEDNVRRMLSTAFALQGFETHCANNGRTALHLFADIHPDVVLMDIRMPE
     SSSSSS   HHHHHHHHHHHH  SSSSS  HHHHHHHHHH    SSSS
MDGIKALKEMRSHETRTPVILMTAYAEVETAVEALRCGAFDYVIKPFDLDELNLIVQRAL
  HHHHHHHHHH    SSSSSS     HHHHHHHH   SSS      HHHHHHHHHH
QLQSMKKEIRHLHQALSTSWQWGHILTNSPAMMDICKDTAKIALSQASVLISGESGTGKE
HHHHHHH    HHHH             HHHHHHH   HHHH    SSSSSS     HH
LIARAIHYNSRRAKGPFIKVNCAALPESLLESELFGHEKGAFTGAQTLRQGLFERANEGT
HHHH       HH    SSSSS    HHHHHHHH                  HHH    S
LLLDEIGEMPLVLQAKLLRILQEREFERIGGHQTIKVDIRIIAATNRDLQAMVKEGTFRE
SSSSS      HHHHHHHHH  SSS         SSS  SSSSSS   HHHHHHH    H
DLFYRLNVIHLILPPLRDRREDISLLANHFLQKFSSENQRDIIDIDPMAMSLLTAWSWPG
HHHHHH  SSSSS       HHHHHHHHHHHHHHHHH          HHHHHHHH
NIRELSNVIERAVVMNSGPIISEDLPPQIRQPVCNAGEVKTAPVGERNLKEEIKRVEKRI
HHHHHHHHHHHHH                 HHHHHHHHH       HHH
IMEVLEQQEGNRTRTALMLGISRRALMYKLQEYGIDPADV
HHHHHHHHHHHHH             HHHHH
```

Fig. 2. The secondary structure of the AtoC model (H: α-helix, S: β-strand). Yellow represents the sequence modelled according to the crystal structure of the σ^{54} activator from *A. aeolicus*. In cyan the DNA binding domain modelled according to the crystal structure of the factor for inversion stimulation from *E. coli* is shown, while green is coloured the structure-less arm linking the domains. (For interpretation of the references to color in this figure legend, the reader is referred to the web version of this article.)

Table 1
Residues in the binding interface between monomers C and D[a].

Residue number	Residue name	Residue number	Residue name	Residue number	Residue name	Residue number	Residue name
Chain C							
6	ARG	118	ARG	200	VAL	273	GLN
30	GLU	121	GLN	201	ASN	274	THR
44	PHE	122	LEU	203	ALA	275	ILE
45	ALA	124	SER	204	ALA	276	LYS
46	ASP	125	MET	205	LEU	277	VAL
47	ILE	126	LYS	209	LEU	287	ARG
48	HIS	127	LYS	213	GLU	333	LYS
72	SER	128	GLU	218	GLU	334	PHE
73	HIS	129	ILE	219	LYS	336	SER
74	GLU	130	ARG	228	LEU	337	GLU
75	THR	131	HIS	229	ARG	338	ASN
76	ARG	132	LEU	230	GLN	339	GLN
92	VAL	134	GLN	232	LEU	356	TRP
95	LEU	135	ALA	234	GLU	359	PRO
96	ARG	136	LEU	235	ARG	360	GLY
100	PHE	139	SER	237	ASN	363	ARG
101	ASP	140	TRP	245	GLU	364	GLU
102	TYR	175	SER	248	GLU	367	ASN
109	LEU	196	PRO	259	ARG	370	GLU
110	ASP	197	PHE	265	GLU	371	ARG
111	GLU	198	ILE	268	ARG	374	VAL
114	LEU	199	LYS	272	HIS	375	MET
Chain D							
30	GLU	122	LEU	201	ASN	285	THR
45	ALA	124	SER	203	ALA	286	ASN
46	ASP	125	MET	204	ALA	287	ARG
47	ILE	126	LYS	212	SER	333	LYS
48	HIS	127	LYS	213	GLU	334	PHE
50	ASP	128	GLU	218	GLU	336	SER
72	SER	129	ILE	219	LYS	337	GLU
73	HIS	130	ARG	228	LEU	338	ASN
74	GLU	131	HIS	229	ARG	339	GLN
75	THR	132	LEU	230	GLN	356	TRP
76	ARG	134	GLN	231	GLY	357	SER
92	VAL	135	ALA	232	LEU	358	TRP
95	LEU	136	LEU	234	GLU	359	PRO
96	ARG	138	THR	235	ARG	360	GLY
99	ALA	139	SER	237	ASN	363	ARG
100	PHE	140	TRP	245	GLU	364	GLU
101	ASP	141	GLN	248	GLU	367	ASN
102	TYR	175	SER	268	ARG	370	GLU
107	PHE	180	GLU	272	HIS	371	ARG
110	ASP	184	ARG	273	GLN	374	VAL
111	GLU	196	PRO	274	THR	375	MET
114	LEU	197	PHE	275	ILE		
118	ARG	198	ILE	276	LYS		

[a] The DBD is not included.

identification of residues located at the interface between AtoC monomers, as well as of residues at the interface between protein and DNA will be very useful for the planning of further experiments, which can either confirm or reject our proposed models.

According to our model the dimer of the aa 6–384 domain is almost symmetric with a twofold axis (↑) along the binding interface (Fig. 3). A large binding interface is formed between the subunits consisting of 88 (chain C) and 94 (chain D) residues (35% non polar) (Table 1). Forty-nine hydrogen bonds and 120 salt bridges as identified by ProtorP [24] stabilize this part of the complex (Table 2). The binding interface between the subunits in the DBD (aa 394–454) consists of 19 (chain C) and 17 (chain D) residues listed in Table 3. The properties of the interface of the whole complex as calculated by ProtorP are summarized in Table 4.

The dimerization binding free energy has been calculated using the program DCOMPLEX (24) to be $\Delta G_{AtoC} = -59.713$ kcal/mol, while the corresponding value for the DBDs part is $\Delta G_{DBD} = -10.226$ kcal/mol.

3.3. Experimental verification of AtoC oligomerization potential

Response regulators are widely considered to bind as dimers to DNA, as previously reported. The ability of AtoC to form dimers/oligomers *in vitro* was here determined by glutaraldehyde cross-linking of its recombinant, purified His-tagged form. Western blot analysis of the products of such, time course, cross-linking experiments indicated that AtoC indeed oligomerized, forming mainly dimers and, though to a much lesser extend, a heterogeneous multimeric population (Fig. 4). The specificity of the cross-linking was assessed by performing parallel reactions with the monomeric protein bovine serum albumin where no formation of non-specific complexes took place under the exact experimental conditions of cross-linking time and glutaraldehyde concentration (data not shown).

3.4. Properties of the DNA model

After equilibration with MDS the DNA model shows significant structural changes (Fig. 5b). Both ends of the double helix are dras-

Table 2
Twenty most important electrostatic attractive and repulsive interactions[a].

Attractive				Repulsive			
Chain C		Chain D		Chain C		Chain D	
Residue number	Residue name	Residue number	Residue name	Residue number	Residue name	Residue number	Residue name
337	GLU	363	ARG	74	GLU	234	GLU
371	ARG	364	GLU	333	LYS	199	LYS
110	ASP	96	ARG	128	GLU	238	GLU
364	GLU	371	ARG	244	ASP	337	GLU
127	LYS	234	GLU	337	GLU	244	ASP
276	LYS	29	GLU	118	ARG	118	ARG
265	GLU	6	ARG	130	ARG	235	ARG
96	ARG	110	ASP	259	ARG	6	ARG
118	ARG	101	ASP	265	GLU	30	GLU
363	ARG	370	GLU	110	ASP	93	GLU
234	GLU	76	ARG	93	GLU	110	ASP
76	ARG	234	GLU	263	GLU	30	GLU
370	GLU	363	ARG	128	GLU	128	GLU
363	ARG	337	GLU	74	GLU	218	GLU
74	GLU	268	ARG	101	ASP	101	ASP
235	ARG	128	GLU	268	ARG	76	ARG
219	LYS	72	SER	76	ARG	268	ARG
30	GLU	276	LYS	333	LYS	363	ARG
337	GLU	199	LYS	6	ARG	276	LYS
72	SER	219	LYS	276	LYS	6	ARG

[a] Interactions are calculated by FastContact (25). The DBD is not included.

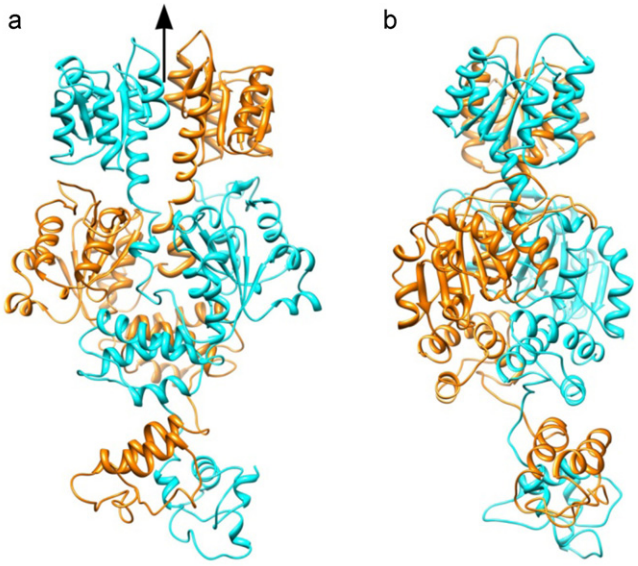

Fig. 3. Two perspectives of the AtoC dimer model rotated by 90°.

tically distorted in a range of about four nucleotide pairs. Similar effects have been reported in earlier MDS studies [18,12]. In order to proceed to a quantitative description and comparison of these structures we ignored the distorted ends of the double helix. The backbone RMSD (root mean squared deviations) of the equilibrated model relative to the starting model was 5.570 Å, while AtoC binding caused a farther increase in RMSD (6.693 Å). Table 5 shows some of the geometrical parameters that characterize the DNA model in its three states as calculated by the program 3DNA. About 57% of the nucleotide pairs of the equilibrated model participate in a B form, while after AtoC binding only 18% preserved the B form. Influence of protein binding on the structure of DNA has been indicated by crystallographic studies in the case of NarL response regulator binding to DNA [16].

Table 3
Properties of the dimer interface.

Properties of interface	
Interface accessible surface area (Å^2)	4839
% Interface accessible surface area	18.8
Residues in interface	117
% Polar residues in interface	29.9
% Non-polar residues in interface	32.5
% Charged residues in interface	37.6
Hydrogen bonds	65
Salt bridges	166

3.5. *Properties of the AtoC–DNA model*

As pointed out in "Section 2", four docking models representing the interaction between DNA and the DBD have been chosen as those satisfying the condition that positions −140, −121 and −111 might be important for AtoC binding. Each of them has been energy minimized and equilibrated for ∼18 ns. At the end of the equilibra-

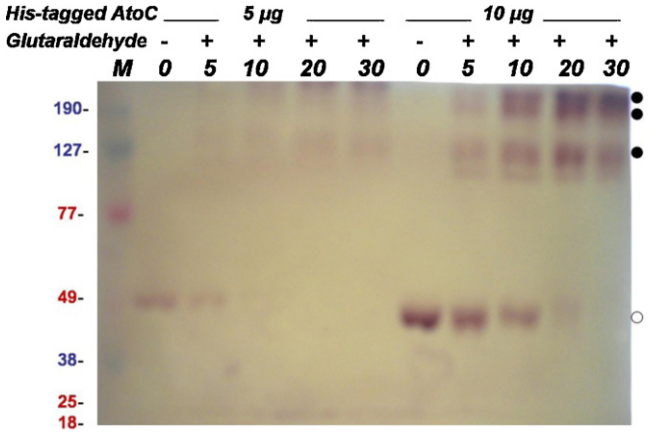

Fig. 4. *In vitro* AtoC oligomerization via chemical cross-linking. Two concentrations of purified His-tagged AtoC were cross-linked with glutaraldehyde 0.1% (v/v) for various times (5, 10, 20 and 30 min). All samples, including non-glutaraldehyde treated controls were subjected to SDS-PAGE 8.5% (w/v) and immunostained with anti-His probe (dilution 1:500). Solid circles stand for oligomers, open for AtoC monomers. Pre-stained protein markers were electrophorized to determine molecular weights: 190, 127: blue, 77, 49: red, 38: blue, 25, 18: red. (For interpretation of the references to color in this figure legend, the reader is referred to the web version of this article.)

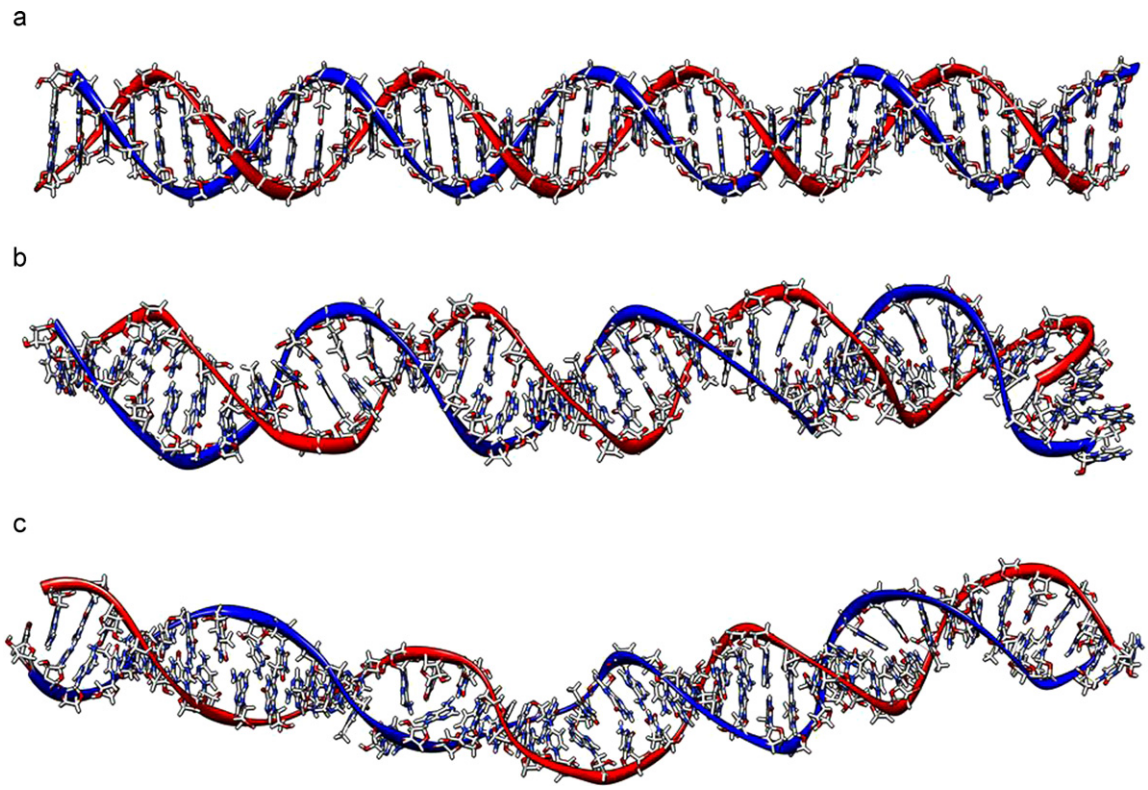

Fig. 5. (a) Starting B-DNA model. (b) The B-DNA model distorted after equilibration with MDS. (c) The same model equilibrated after binding to AtoC adopting a curved conformation.

tion, all four models have shown a more or less similar bending of DNA caused by the protein interaction. Among the four equilibrated models the one with minimum protein–DNA interaction energy has been adopted as the model representing the AtoC–DNA interaction. The later has been used to construct a model of two DBDs bound to DNA (satisfying the above mentioned conditions) (Fig. 6), which has been then further minimized and equilibrated for 3 ns.

One DBD binds in the major groove defined by nucleotides C19 (strand A) and C17 (strand B), while the other between A20 (strand A) and G16 (strand B). The binding interface of the first DBD is defined by residues Glu399, Thr402, Val405, Gly406, Glu407, Arg408, Asn409, Leu410, Lys411, Glu412, Glu413, Ser443, Arg445, Ala446, Leu447, Met448, Tyr449, and Lys450, which make direct contacts to DNA. On the other hand the second DBD interacts with DNA with residues Gly398, Lys401, Thr402, Pro404, Val405, Gly406, Glu407, Arg408, Asn409, Leu410, Lys411, Glu412, Glu413, Ala437, Leu438, Ile442, Ser443, Arg445 and Ala446. As expected both protein interfaces consist mostly (72%) of identical residues.

The first DBD interacts with A14, T15, G16, C17, A18, C19 and A20 of strand A and with G18, C19, A20, C21, T22, G23 and T24 of strand B. The second one interacts with C19, A20, G21, T22, G23, C24, G25 and C26 of strand A and with T15, G16, C17, G18, C19 and A20 of strand B.

The binding of DBD to DNA does not only affect the conformation of DNA, but also leads to significant structural changes to the DBD itself as it is illustrated in Fig. 7. The binding free energy between the two DBDs and DNA from our equilibrated model was calculated by DDNA2 (25) to be $\Delta G_{\text{bd-DNA}} = -14.161$ kcal/mol, a value significantly lower than that of the binding energy between the domains themselves ($\Delta G_{\text{DBD}} = -10.226$ kcal/mol). This suggests a propensity for the formation of stable AtoC–DNA complexes. The DBDs do not have to completely dissociate before they bind to DNA, since the binding sites are different in the two cases. Probably one of the DBDs binds to DNA changing its conformation a fact that destabilizes locally the dimer allowing for further binding of the second DBD.

Fig. 6. Model of two AtoC DNA binding domains bound to DNA.

Table 4
Residues in the binding interface between monomers C and D in the DBD.

Chain C		Chain D	
Residue number	Residue name	Residue number	Residue name
394	VAL	394	VAL
395	CYS	395	CYS
396	ASN	398	GLY
397	ALA	399	GLU
398	GLY	402	THR
399	GLU	403	ALA
401	LYS	407	GLU
402	THR	408	ARG
405	VAL	410	LEU
406	GLY	413	GLU
431	GLY	416	ARG
434	THR	417	VAL
435	ARG	418	GLU
436	THR	419	LYS
437	ALA	420	ARG
438	LEU	421	ILE
441	GLY	424	GLU
443	SER		
444	ARG		

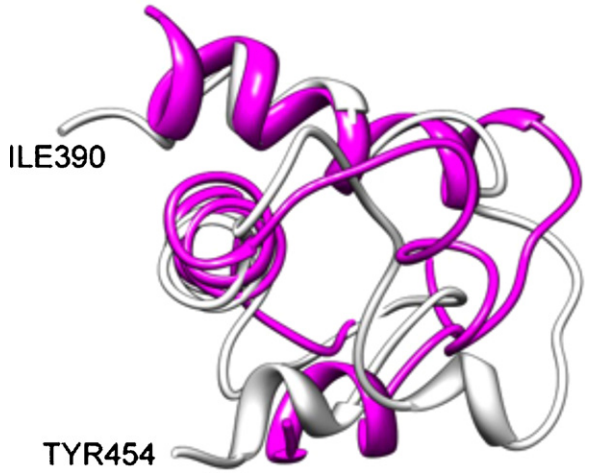

Fig. 7. The DNA binding domains in its dimer (*grey*) and DNA binding (*magenta*) conformation bearing large conformational changes. (For interpretation of the references to color in this figure legend, the reader is referred to the web version of this article.)

4. Discussion

AtoC response regulator has been found to exhibit characteristic functions shared between prokaryotic transcriptional regulators like NtrC, while the AtoSC two-component system is mentioned in the same line with other multi-functional *E. coli* two component systems. Following acetoacetate sensing, the AtoS kinase phosphorylates AtoC on its receiver domain, while the AtoC central domain possesses ATPase activity, and its HTH domain is responsible for binding to DNA. These properties, attributed to AtoC according to its homology with known regulators at first, have been experimentally verified or partially visualized by 3D comparative modelling. Nevertheless, the issue of AtoC oligomerization remained vague, while never before a model of the AtoC protein as a whole, let alone in its putative dimerization state was presented, and the present study aimed towards filling this void. Our next goal was to gain a deeper insight to the interactions that govern already characterized properties such as AtoC binding to DNA.

In silico methods, correlating protein and DNA sequences and structures to their function are commonly implemented in order to elucidate the mechanisms of phosphotransfer, DNA-binding and oligomerization. Since AtoC has not yet been crystallized, albeit repeated efforts, to address these issues we used the docking strategy and Molecular Dynamics Simulations in order to predict protein, DNA and their complex structures.

Table 5
Geometrical properties of the equilibrated DNA model before and after AtoC binding[a].

Mean values over the double helix length	Starting B-DNA model	Equilibrated model before AtoC binding	Equilibrated model after AtoC binding
Form [% B]	100	56.8	18.2
Propeller [°]	4.0	−19.2	−12.8
Tilt [°]	0.0	0.81	−0.6
Roll [°]	−3.6	10.3	8.2
h-rise [Å]	3.4	3.2	3.1
h-twist [deg]	36.1	33.5	30.8
Minor groove [Å]	11.7	13.7	15.6
Major groove [Å]	17.0	18.1	18.5
Helix radius [Å]	8.9	9.9	9.6

[a] For the geometrical parameters of DNA the nomenclature and the conventions of the 3DNA program are adopted. Properties are calculated by the 3DNA program.

The almost complete AtoC model (Fig. 1), including its DBD, was derived by merging its structural fragments which were separately modelled according to their homology to protein domains with already derived structures, followed by MDS equilibration. We implemented the same approach in order to construct a model of an AtoC dimer. The two aforementioned domains were separately modelled as partial dimers and then rebuilt in one, joined together by the structure-less arm highlighted in Fig. 3, while its structural properties were calculated. An almost symmetric dimer is formed by aa 6–384 with a twofold axis (↑) along a large binding interface (Fig. 3) consisting of 88 (chain C) and 94 (chain D) residues (only 35% non polar) (Table 1). The dimerization binding free energy has been calculated to be $\Delta G_{AtoC} = -59.713$ kcal/mol, while the DBDs part contributes with −10.226 kcal/mol. Furthermore, we provide for the first time experimental evidence of the AtoC ability to form dimers and oligomers, as Fig. 7 demonstrates.

A B-DNA 3D model of the inverted palindrome, comprising the AtoC binding target in the *atoDAEB* operon, was constructed and equilibrated by MDS, exhibiting several structural distortions, also reported in cases of other regulators binding to DNA. The equilibrated B-DNA model retained 56.8% of its structure in B form. Docking of the AtoC DBD to the B-DNA structure seems to force drastic changes to the B-form, a feature common to such activator–DNA interactions (Figs. 5 and 6). In this case only 18.2% of the DNA was in B form after equilibration. Influence of protein binding on the structure of DNA has been reported by crystallography in the case of NarL response regulator binding to DNA [16]. Moreover, binding of the DBD to DNA does not seem to affect only the DNA conformation, but also leads to significant structural changes of the DBD itself as it is illustrated in Fig. 7. Response regulators are reported to bind to their target sequences in the form of dimers, and our data provide strong evidence that this is also the case with AtoC, in the scenario of two DBDs docking to the B-DNA structure of the inverted palindrome. Since the DBDs bind DNA with $\Delta G_{bd\text{-}DNA} = -14.161$ kcal/mol and the binding energy between the domains themselves is $\Delta G_{DBD} = -10.226$ kcal/mol, it can be concluded that AtoC forms stable AtoC–DNA complexes. The DBDs do not have to completely dissociate before they bind to DNA, since the binding sites are different in the two cases. One of the DBDs might bind to DNA changing its conformation a fact that destabilizes locally the dimer allowing for further binding of the second DBD.

5. Conclusion

In conclusion, the present study has provided a first step towards understanding the mechanism in which the AtoC response regulator functions as a transcriptional activator, while predicting complex structures of protein–DNA.

References

[1] S. Arnott, P.J. Campbell-Smith, R. Chandrasekaran, Nucleic acids—volume II, in: G.P. Fasman (Ed.), Handbook of Biochemistry and Molecular Biology, 3rd ed., CRC Press, Cleveland, 1976, pp. 411–422.

[2] H. Barrios, B. Valderrama, E. Morett, Compilation and analysis of sigma^{54}-dependent promoter sequences, Nucleic Acids Res. 27 (1999) 4305–4313.

[3] C.J. Camacho, C. Zhang, FastContact: rapid estimate of contact and binding free energies, Bioinformatics 21 (2005) 2534–2536.

[4] P.S. Filippou, L.D. Kasemian, C.A. Panagiotidis, D.A. Kyriakidis, Functional characterization of the histidine kinase of the *E. coli* two-component signal transduction system AtoSC, Biochim. Biophys. Acta 1780 (2008) 1023–1031.

[5] Y. Flashner, D.S. Weiss, J. Keener, S. Kustu, Constitutive forms of the enhancer-binding protein NtrC: evidence that essential oligomerization determinants lie in the central activation domain, J. Mol. Biol. 249 (1995) 700–713.

[6] A.I. Grigoroudis, C.A. Panagiotidis, E.E. Lioliou, M. Vlassi, D.A. Kyriakidis, Molecular modeling and functional analysis of the AtoS–AtoC two-component signal transduction system of *Escherichia coli*, Biochim. Biophys. Acta 1770 (2007) 1248–1258.

[7] X. Huang, W. Miller, Adv. Appl. Math. 12 (1991) 373–381.

[8] W. Humphrey, A. Dalke, K. Schulten, VMD: visual molecular dynamics, J. Mol. Graph. 14 (33–38) (1996) 27–28.

[9] L.S. Jenkins, W.D. Nunn, Regulation of the ato operon by the AtoC gene in *Escherichia coli*, J. Bacteriol. 169 (1987) 2096–2102.

[10] D.T. Jones, Protein secondary structure prediction based on position-specific scoring matrices, J. Mol. Biol. 292 (1999) 195–202.

[11] L.A. Kelley, M.J.E. Sternberg, Protein structure prediction on the web: a case study using the Phyre server, Nat. Protoc. 4 (2009) 363–371.

[12] Y. Komeiji, M. Uebayasi, Change in conformation by DNA–peptide association: molecular dynamics of the hin-recombinase–hixL complex, Biophys. J. 77 (1999) 123–138.

[13] D.A. Kyriakidis, M.C. Theodorou, P.S. Filippou, K.D. Kyriakidis, E. Tiligada, Effect of histamine on the signal transduction of the AtoS–AtoC two component system and involvement in poly-(R)-3-hydroxybutyrate biosynthesis in *Escherichia coli*, Amino Acids 35 (2008) 45–52.

[14] E.E. Lioliou, E.P. Mimitou, A.I. Grigoroudis, C.H. Panagiotidis, C.A. Panagiotidis, D.A. Kyriakidis, Phosphorylation activity of the response regulator of the two-component signal transduction system AtoS–AtoC in *E. coli*, Biochim. Biophys. Acta 1725 (2005) 257–268.

[15] S. Liu, C. Zhang, H. Zhou, Y. Zhou, A physical reference state unifies the structure-derived potential of mean force for protein folding and binding, Proteins 56 (2004) 93–101.

[16] E.A. Maris, M.R. Sawaya, M. Kaczor-Grzeskowiak, M.R. Jarvis, S.M.D. Bearson, M.L. Kopka, I. Schröder, R.P. Gunsalus, R.E. Dickerson, Dimerization allows DNA target site recognition by the NarL response regulator, Nat. Struct. Biol. 9 (2002) 771–778.

[17] M.K. Matta, E.E. Lioliou, C.H. Panagiotidis, D.A. Kyriakidis, C.A. Panagiotidis, Interactions of the antizyme AtoC with regulatory elements of the *Escherichia coli* atoDAEB operon, J. Bacteriol. 189 (2007) 6324–6332.

[18] O. Noberto de Souza, R.L. Ornstein, Effect of warmup protocol and sampling time on convergence of molecular dynamics simulations of a DNA dodecamer using AMBER 4. 1 and particle-mesh Ewald method, J. Biomol. Struct. Dyn. 14 (1997) 607–611.

[19] T. Oshima, H. Aiba, Y. Masuda, S. Kanaya, M. Sugiura, B.L. Wanner, H. Mori, T. Mizuno, Transcriptome analysis of all two-component regulatory system mutants of *Escherichia coli* K-12, Mol. Microbiol. 46 (2002) 281–291.

[20] G. Pauli, P. Overath, Ato operon: a highly inducible system for acetoacetate and butyrate degradation in *Escherichia coli*, Eur. J. Biochem. 29 (1972) 553–562.

[21] E.F. Pettersen, T.D. Goddard, C.C. Huang, G.S. Couch, D.M. Greenblatt, E.C. Meng, T.E. Ferrin, UCSF Chimera—a visualization system for exploratory research and analysis, J. Comput. Chem. 25 (2004) 1605–1612.

[22] J.C. Phillips, R. Braun, W. Wang, J. Gumbart, E. Tajkhorshid, E. Villa, C. Chipot, R.D. Skeel, L. Kale, K. Schulten, Scalable molecular dynamics with NAMD, J. Comput. Chem. 26 (2005) 1781–1802.

[23] L. Reitzer, B.L. Schneider, Metabolic context and possible physiological themes of σ^{54}-dependent genes in *Escherichia coli*, Microbiol. Mol. Biol. Rev. 65 (2001) 422–444.

[24] C. Reynolds, D. Damerell, S. Jones, ProtorP: a protein–protein interaction analysis server, Bioinformatics (Structural Bioinformatics) 25 (2009) 413–414.

[25] D.W. Ritchie, parametric protein shape recognition, Dissertation, University of Aberdeen, 1998.

[26] T. Schwede, J. Kopp, N. Guex, M.C. Peitsch, SWISS-MODEL: an automated protein homology-modeling server, Nucleic Acids Res. 31 (2003) 3381–3385.

[27] A.M. Stock, V.L. Robinson, P.N. Goudreau, Two-component signal transduction, Annu. Rev. Biochem. 69 (2000) 183–215.

[28] M.C. Theodorou, C.A. Panagiotidis, C.H. Panagiotidis, A.A. Pantazaki, D.A. Kyriakidis, Involvement of the AtoS–AtoC signal transduction system in poly-(R)-3-hydroxybutyrate biosynthesis in *Escherichia coli*, Biochim. Biophys. Acta 1760 (2006) 896–906.

[29] M.C. Theodorou, E.C. Theodorou, C.A. Panagiotidis, D.A. Kyriakidis, Spermidine triggering effect to the signal transduction through the AtoS–AtoC/Az two-component system in *Escherichia coli*, Biochim. Biophys. Acta 1770 (2007) 1104–1114.

[30] B. Wallner, A. Elofsson, Can correct protein models be identified, Protein Sci. 12 (5) (2003) 1073–1086.

[31] A.B. Wedel, S. Kustu, The bacterial enhancer-binding protein NTRC is a molecular machine: ATP hydrolysis is coupled to transcriptional activation, Genes Dev. 19 (1995) 2042–2052.

[32] A.H. West, A.M. Stock, Histidine kinases and response regulator proteins in two-component signaling systems, Trends Biochem. Sci. 26 (2001) 369–376.

[33] L. Xiang-Jun, W.K. Olson, 3DNA: a software package for the analysis, rebuilding and visualization of three-dimensional nucleic acid structures, Nucleic Acids Res. 31 (2003) 5108–5121.

[34] B. Xu, Y. Yang, H. Liang, Y. Zhou, An all-atom knowledge-based energy function for protein–DNA threading, decoy discrimination, and prediction of transcription-factor binding profiles, Proteins: Struct. Funct. Bioinform. 76 (2009) 718–730.

[35] X.F. Yang, Y. Ji, B.L. Schneider, L. Reitzer, Phosphorylation-independent dimer–dimer interactions by the enhancer-binding activator NtrC of *Escherichia coli*: a third function for the C-terminal domain, J. Biol. Chem. 279 (2004) 36708–36714.

[36] X. Zhang, M. Chaney, S.R. Wigneshweraraj, J. Schumacher, P. Borders, W. Cannon, M. Buck, Mechanochemical ATPases and transcriptional activation, Mol. Microbiol. 45 (2002) 895–903, http://bioinf.cs.ucl.ac.uk/psipred/.